Infrared absorption of methanethiol clusters (CH3SH) n , n = 2–5, recorded with a time-of-flight mass spectrometer using IR depletion and VUV ionization

Lung Fu, Hui-Ling Han, and Yuan-Pern Lee

Articles you may be interested in

Photodissociation of (SO2XH) Van der Waals complexes and clusters (XH = C2H2, C2H4, C2H6) excited at 32 040–32090 cm1 with formation of HSO2 and X
J. Chem. Phys. **140**, 054304 (2014); 10.1063/1.4863445

Experimental and theoretical studies of neutral Mg m C n H x and Be m C n H x clusters
J. Chem. Phys. **135**, 054307 (2011); 10.1063/1.3617571

Methanol clusters (CH3OH) n , n = 3–6 in external electric fields: Density functional theory approach
J. Chem. Phys. **135**, 024307 (2011); 10.1063/1.3605630

Infrared absorption of methanol clusters (CH3OH) n with n = 26 recorded with a time-of-flight mass spectrometer using infrared depletion and vacuum-ultraviolet ionization
J. Chem. Phys. **134**, 144309 (2011); 10.1063/1.3572225

IR plus vacuum ultraviolet spectroscopy of neutral and ionic organic acid molecules and clusters: Acetic acid
J. Chem. Phys. **125**, 184308 (2006); 10.1063/1.2378626

Infrared absorption of methanethiol clusters (CH$_3$SH)$_n$, n = 2–5, recorded with a time-of-flight mass spectrometer using IR depletion and VUV ionization

Lung Fu,[1] Hui-Ling Han,[1] and Yuan-Pern Lee[1,2,a)]

[1]*Department of Applied Chemistry and Institute of Molecular Science, National Chiao Tung University, Hsinchu 30010, Taiwan*
[2]*Institute of Atomic and Molecular Sciences, Academia Sinica, Taipei 10617, Taiwan*

We investigated IR spectra in the CH- and SH-stretching regions of size-selected methanethiol clusters, (CH$_3$SH)$_n$ with n = 2–5, in a pulsed supersonic jet using infrared (IR)-vacuum ultraviolet (VUV) ionization. VUV emission at 132.50 nm served as the source of ionization in a time-of-flight mass spectrometer. Clusters were dissociated with light from a tunable IR laser before ionization. The variations in intensity of methanethiol cluster ions (CH$_3$SH)$_n^+$ were monitored as the IR laser light was tuned across the range 2470–3100 cm^{-1}. In the SH-stretching region, the spectrum of (CH$_3$SH)$_2$ shows a weak band near 2601 cm^{-1}, red-shifted only 7 cm^{-1} from that of the monomer. In contrast, all spectra of (CH$_3$SH)$_n$, n = 3–5, show a broad band near 2567 cm^{-1} with much greater intensity. In the CH-stretching region, absorption bands of (CH$_3$SH)$_2$ are located near 2865, 2890, 2944, and 3010 cm^{-1}, red-shifted by 3–5 cm^{-1} from those of CH$_3$SH. These red shifts increase slightly for larger clusters and bands near 2856, 2884, 2938, and 3005 cm^{-1} were observed for (CH$_3$SH)$_5$. These spectral results indicate that the S–H$\cdots$S hydrogen bond plays an important role in clusters with n = 3–5, but not in (CH$_3$SH)$_2$, in agreement with theoretical predictions. The absence of a band near 2608 cm^{-1} that corresponds to absorption of the non-hydrogen-bonded SH moiety and the large width of observed feature near 2567 cm^{-1} indicate that the dominant stable structures of (CH$_3$SH)$_n$, n = 3–5, have a cyclic hydrogen-bonded framework. © *2012 American Institute of Physics.* [http://dx.doi.org/10.1063/1.4770227]

I. INTRODUCTION

Vibrational spectra provide an important means to analyze the structures of hydrogen-bonded clusters and their intermolecular interactions.[1–3] Methanol clusters, (CH$_3$OH)$_n$, have been much investigated[4,5] through their infrared (IR) spectra.[6–13] The published experimental results indicate that (CH$_3$OH)$_2$ has an open-chain structure, whereas cyclic hydrogen-bonded structures dominate in larger clusters of CH$_3$OH.[11–13]

Compared with oxygen, sulfur is less electronegative, and hence a poor proton acceptor in hydrogen bond. Although there is evidence that the O–H$\cdots$S (Ref. 14) and the S–H$\cdots$S hydrogen bonds exist in solids,[15] experimental investigations on the hydrogen bonding systems involving S atoms are scarce. Wategaonkar and co-workers investigated O–H$\cdots$O versus O–H$\cdots$S hydrogen bonding systems through experimental and theoretical studies on the complexes of *p*-cresol with H$_2$O or H$_2$S,[16] and with alcohols and thiols.[17] They found that the sulfur atom acts as the OH hydrogen bond acceptor, but with interaction energy about half that of the oxygen atom.

Methanethiol (CH$_3$SH), the smallest thiol, exists in the blood of human beings and animals and in the tissues

of plants.[18] Experimental investigations of the clusters of CH$_3$SH are limited. Barnes *et al.* employed matrix isolation techniques and observed, in addition to the band at 2603 cm^{-1} for CH$_3$SH, a band near 2576 cm^{-1} assigned to an open-chain dimer and a band near 2550 cm^{-1} to the cyclic tetramer.[19] Odutola *et al.* employed a molecular beam and electric deflection to report that (CH$_3$SH)$_2$ and (CH$_3$SH)$_3$ are both polar,[20] in contrast to the case of methanol clusters in which (CH$_3$OH)$_2$ is polar whereas (CH$_3$OH)$_3$ is non-polar.[4] The reason is that (CH$_3$OH)$_2$ has an open-chain structure, whereas (CH$_3$OH)$_3$ has a cyclic hydrogen-bonding framework.

Several groups have investigated CH$_3$SH clusters with various computational methods.[21–25] Sum and Sandler employed the MP2/aug-cc-pVDZ method and reported that CH$_3$SH clusters exhibit no cooperative effect as CH$_3$OH clusters, and concluded that no S–H$\cdots$S hydrogen bond is present in CH$_3$SH clusters.[22] Bakó and Pálinkás employed the MP2/6-311+G** method and obtained two stable structures of (CH$_3$SH)$_2$; the one with the S–H$\cdots$S hydrogen bond has energy greater than the one without hydrogen bonding by ~2 kJ mol^{-1}.[23] Cabaleiro-Lago and Rodríguez-Otero employed the Hartree-Fock (HF), density functional theory (DFT), and Møller–Plesset perturbation (MP2) methods with the aug-pVDZ/cc-pVDZ basis set from which the diffuse functions of H atoms were excluded; they found five stable structures of (CH$_3$SH)$_2$ and (CH$_3$SH)$_3$, as reproduced in Figs. 1 and 2, respectively.[24] For (CH$_3$SH)$_2$, the most

---

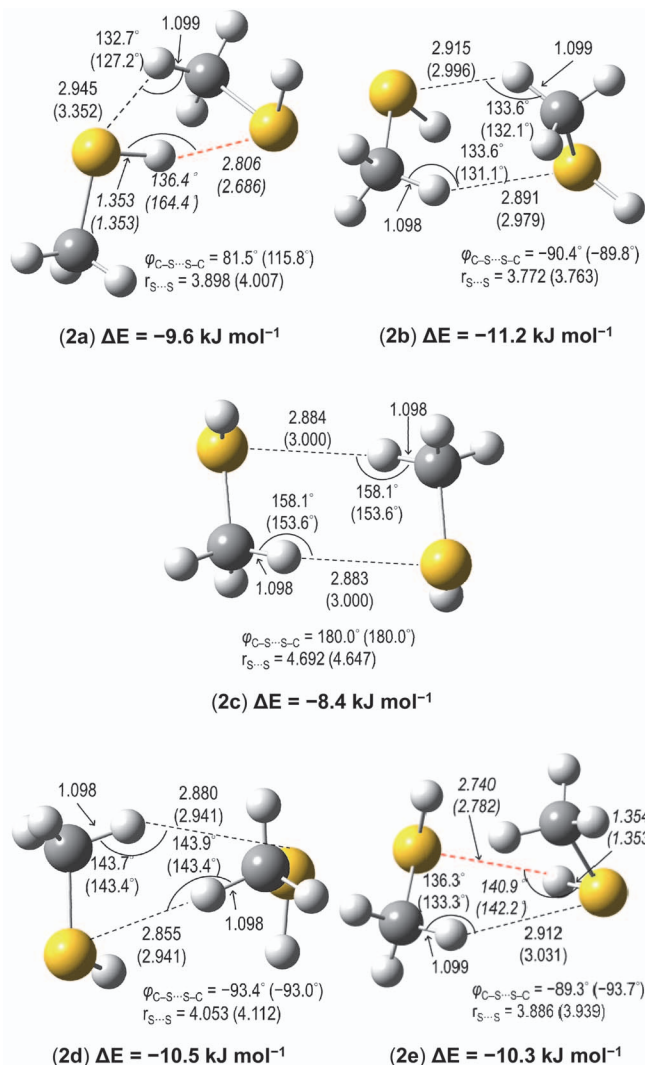a)Author to whom correspondence should be addressed. Electronic mail: yplee@mail.nctu.edu.tw. FAX: 886-3-5713491.

FIG. 1. Geometries of $(CH_3SH)_2$ predicted with the MP2/aug-cc-pVDZ method. Representative parameters predicted by Cabaleiro-Lago and Rodríguez-Otero[24] with the B3LYP/aug-cc-pVDZ method are listed in parentheses. The S–H $\cdots$ S hydrogen bond is indicated with a red dashed line; other non-valence interactions are indicated with black dashed lines. Bond distances are in Å and angles in degree. The literature stabilization energies relative to monomers are also listed.[24]

FIG. 2. Geometries of $(CH_3SH)_3$ predicted by Cabaleiro-Lago and Rodríguez-Otero[24] with the B3LYP/aug-cc-pVDZ method (parameters listed in parentheses) and that of structure (**3c**) predicted with the MP2/aug-cc-pVDZ method. The S–H $\cdots$ S hydrogen bond is indicated with a red dashed line; other non-valence interactions are indicated with black dashed lines. Bond distances are in Å and angles in degree. The literature stabilization energies relative to monomers are also listed.[24]

stable structure (**2b**) with stabilization energy of -11.2 kJ mol^{-1} predicted with the MP2 method has no S–H $\cdots$ S hydrogen bond. The two hydrogen-bonded structures (**2a**) and (**2e**) have energies 1.6 and 0.9 kJ mol^{-1} greater than that of structure (**2b**). These authors predicted also, with the B3LYP method, that the hydrogen-bonded structures are characterized by an enhanced IR absorption of the SH-stretching mode red-shifted by ~ 60 cm^{-1} from that of CH_3SH, whereas the non-hydrogen-bonded ones show small IR intensity and small (< 8 cm^{-1}) shifts. In contrast, all five stable structures of $(CH_3SH)_3$ have S–H $\cdots$ S hydrogen-bonds with bands of the SH-stretching modes shifted 67–87 cm^{-1} to the red.

The IR spectra of molecular clusters of varied sizes are similar and often overlapped with each other. Because clusters are typically generated with a distribution of sizes, without mass selection or mass-specific measurements, to characterize the IR spectrum of clusters of a distinct size is difficult.
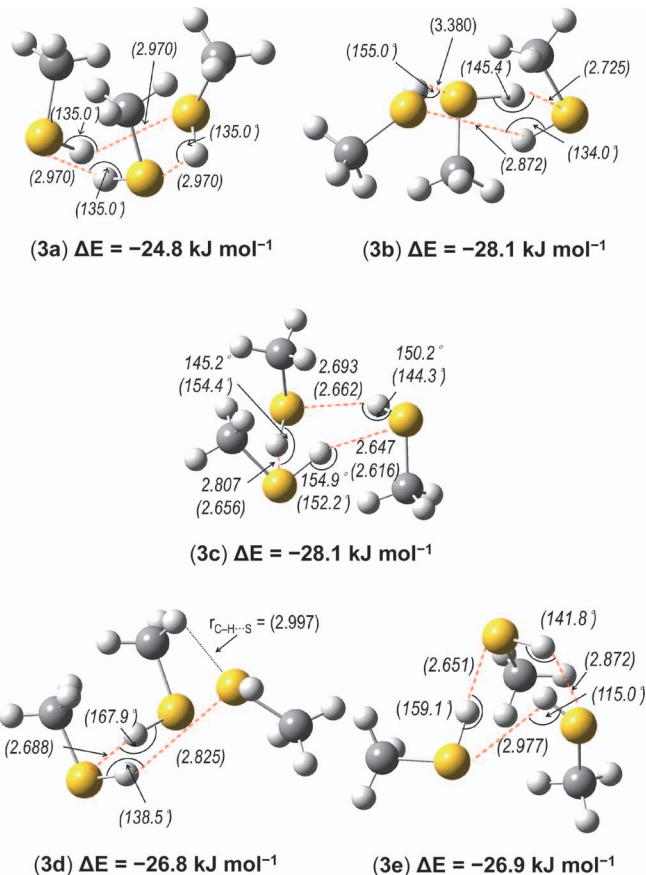
Vibrational excitation and dissociation combined with VUV photoionization enable measurements of vibrational spectra of size-selected neutral clusters.[26] The dissociation of clusters with light from an IR laser can result in a variation of the population distribution of clusters, hence the ion signal of cluster ions induced with VUV light.[6, 7, 27–30] We have applied VUV photoionization and a time-of-flight (TOF) mass spectrometer to detect methanol clusters in a pulsed supersonic jet, and we employed IR laser radiation, tuned through the region 2650–3750 cm^{-1}, to photodissociate methanol clusters. By the careful processing of action spectra according to photoionization efficiencies and a mechanism that took into account the production and loss of each cluster, we obtained the IR spectra of size-selected clusters $(CH_3OH)_n$, $n \le 6$.[13] In the present work, we turned our attention to CH_3SH clusters to obtain IR spectra of $(CH_3SH)_n$, $n \le 5$; we found that the S–H $\cdots$ S hydrogen bond exists only in $(CH_3SH)_n$, $n = 3$–5, but not in $(CH_3SH)_2$, consistent with theoretical predictions.

II. EXPERIMENTS

The apparatus used to perform IR-VUV photoionization spectroscopy is similar to that used in our previous

experiments.[13,31] A pulsed jet of CH_3SH (1%) seeded in Ne was produced on supersonic expansion through a pulsed Even–Lavie valve (10 Hz) with a total stagnation pressure of 3.3 atm. Methanethiol clusters were formed during adiabatic expansion through the nozzle. The gaseous jet was skimmed with a conical skimmer (diameter 1.0 mm) before being introduced into the photoionization region of the TOF mass spectrometer, which was located $\sim$15 cm downstream from the nozzle tip. The pressures in the source and ionization chambers were 1×10^{-6} and 7×10^{-7} Torr, respectively, under typical operating conditions.

The VUV laser light that served as the ionization source was generated through resonant-enhanced four-wave difference-frequency mixing ($\omega_{VUV} = 2\omega_1 - \omega_2$) using a UV and a visible laser beam. The UV light at $\omega_1 = 47\,046.43$ cm^{-1} (212.556 nm), obtained from the second-harmonic output of a dye laser (Scanmate 2E, Lambda Physik), was employed to achieve the two-photon transition of Kr $4p^6(^1S_0)$ $\rightarrow 4p^5(^2P_{3/2})5p(^2[1/2]_0)$. The tunable visible light was generated with a second dye laser (Scanmate 2E, Lambda Physik) with $\omega_2 = 17\,390\text{–}19\,380$ cm^{-1} (516–575 nm). Both UV and visible laser beams were focused into the gas cell containing a mixture of Kr and Ar (1:3 at 50 Torr) with a MgF_2 lens ($f = 20$ cm). The resulting VUV light was separated from the UV and visible beams with a convex MgF_2 lens ($f = 15$ cm) before being introduced into the center of the ionization region. Both dye lasers were pumped with the 355-nm output of a Nd:YAG laser (Spectra Physics, PRO-270, 230 mJ pulse^{-1}, 10 Hz). In most experiments, the visible light was set at $18\,622$ cm^{-1} (537.00 nm) to produce the VUV light at 132.50 nm (9.3572 eV, 75,471 cm^{-1}).

$(CH_3SH)_n$ molecules were ionized in the ionization region of a time-of-flight (TOF) mass spectrometer to form $(CH_3SH)_n^+$, which were extracted perpendicularly with a potential of 200 V and accelerated into a field-free tube (length 1 m). The accelerator and repeller plates of the ion optics were biased at 1500 and 1700 V, respectively. Ions were subsequently detected with a microchannel plate (18 mm, MCP, Burle Electro-Optics). After passing a preamplifier (EG&G ORTEC, Model 9306, bandwidth 1 GHz), the ion signal was recorded with a 14-bit digitizer (GaGe Instruments, CS8327, 100 MS/s) and also displayed on a digital oscilloscope. The digitizer was connected to a computer for data processing and storage.

The tunable emission from an IR laser preceded the VUV laser pulse by $\sim$100 ns to serve as a photodissociation source for the CH_3SH clusters. The IR laser beam was generated with an optical parametric oscillator/amplifier (OPO/OPA) system (LaserVision, resolution $\sim$2.0 cm^{-1} with broadband cavity) that was pumped with a Nd:YAG laser (Continuum, Powerlite 8000, 1064 nm, 460 mJ pulse^{-1}, 10 Hz, injection seeded). The IR beam was focused onto the ionization region with a silver-coated parabolic mirror ($f = 20$ cm), resulting in a spot of size $\sim$1 mm^2 at the photoionization region. The direction of the IR beam was counter-propagating with the VUV beam and perpendicular to the flight path of the drift tube for TOF-MS. The energy before entering the photoionization region increased from 1 mJ at 2470 cm^{-1} to 2.5 mJ at 2670 cm^{-1}, and $\sim$5 mJ in the spectral range of 2800–3100 cm^{-1}. A delay

generator (Berkeley Nucleonics Corporation, BNC-575) controlled the time sequence of the VUV laser, the IR laser, the pulsed valve, and the digitizer.

The ion signals were monitored as the wavenumber of the IR laser was tuned through ranges of 2470–2670 cm^{-1} and 2800–3100 cm^{-1} while the wavelength of the VUV laser was maintained at 132.50 nm, $\sim$716 cm^{-1} below the ionization threshold of CH_3SH monomer and more than 1 eV above the ionization thresholds of the CH_3SH clusters. The wavelength of IR light was calibrated with the photoacoustic spectra of reference gases (CH_4, C_2H_2, or H_2O) recorded simultaneously.

By adjusting the driving current of the pulse valve, we could alter the displacement and opening duration of the valve, hence the size distribution of clusters. Change in stagnation pressure also altered the cluster size distribution. In these experiments, we found that a particular combination of stagnation pressure and driving current could yield our desired size distribution of clusters, to be discussed in the section of experimental results.

III. COMPUTATIONS

All calculations were performed using the GAUSSIAN 09 package.[32] Geometries of five structures of $(CH_3SH)_2$ and the most stable one of $(CH_3SH)_3$ were optimized using second-order Møller–Plesset perturbation (MP2) theory with the aug-cc-pVDZ basis set[33,34] based on the structures reported by Cabaleiro-Lago and Rodríguez-Otero;[24] the criterion of convergence was set to "very tight." The results are shown in Figs. 1 and 2 for $(CH_3SH)_2$ and $(CH_3SH)_3$, respectively; critical parameters are compared with those reported by Cabaleiro-Lago and Rodríguez-Otero (listed parenthetically).

Rotational parameters A, B, and C calculated with the MP2/aug-cc-pVDZ method for the ground and some vibrationally excited states of CH_3SH are listed in Table I. The vector components of the dipole derivative projected onto the molecular axes represent the weighting of the transition types; they are also listed in Table I. Harmonic and anharmonic vibrational wavenumbers and IR intensities of all five structures of $(CH_3SH)_2$ were predicted with the MP2/aug-cc-pVDZ method; those of the SH-stretching and the CH-stretching modes are listed in Tables II and III, respectively. Because of the large size, harmonic vibrational wavenumbers and IR intensities were calculated for only the most stable structure (**3c**) of $(CH_3SH)_3$.

The vertical ionization energy (IE) of CH_3SH is predicted to be 9.46 eV with the Gaussian-3 (G3) method,[35] consistent with the experimental value of 9.446 ± 0.1 eV.[36] The vertical IE of $(CH_3SH)_2$ is predicted to be 8.26 eV for structure (**2b**).

IV. RESULTS AND DISCUSSION

A. TOF mass spectra of methanethiol clusters

We performed experiments under various conditions to produce disparate distributions of CH_3SH clusters. Here, we

TABLE I. Comparison of rotational parameters of CH$_3$SH in their ground and vibrationally excited states predicted with the MP2/aug-cc-pVDZ method.

Mode	A /cm^{-1}	B /cm^{-1}	C /cm^{-1}	a-type/b-type
ν_1 (3015 cm^{-1})	3.33848	0.420005	0.403109	0.00/1.00[a]
ν_2 (2947 cm^{-1})	3.33053	0.419791	0.402957	0.96/0.04
ν_3 (2605 cm^{-1})	3.32047	0.419936	0.402678	0.25/0.75
ν_9 (3012 cm^{-1})	3.33803	0.419928	0.403101	0.29/0.71
$2\nu_4$ (2889 cm^{-1})	3.95206	0.420104	0.406862	0.40/0.60
$2\nu_{10}$ (2864 cm^{-1})	2.69095	0.424919	0.403622	0.00/1.00[a]
Equilibrium	3.38399	0.424297	0.406934	
Ground state	3.35274	0.419925	0.403071	

[a]a-type/c-type.

present results of experiments with three representative cluster distributions.

In experimental condition A, we managed to produce predominantly the dimer cluster by using a stagnation pressure 3.3 atm for CH$_3$SH/Ne (1%) and setting the driving

current of the pulse valve to 96 A. The TOF mass spectrum of methanethiol cluster ions induced with VUV ionization at 132.50 nm is shown in Fig. 3(a); assignments of mass signals according to ratio of mass to charge (m/z) are also indicated. Dimeric methanethiol cluster ion (CH$_3$SH)$_2^+$, $m/z = 96$ and indicated as M$_2^+$ in Fig. 3(a), is the dominant species. A small signal of CH$_3$SH$^+$, indicated as M$^+$, is likely due to the Penning ionization of CH$_3$SH; the IE of CH$_3$SH is 9.446 eV, greater than the VUV photon energy 9.3572 eV employed. The IE of (CH$_3$SH)$_n$, $n \geq 2$, are expected to be smaller than 8.5 eV, such as 8.26 eV predicted for (CH$_3$SH)$_2$. Under this experimental condition, cations corresponding to clusters (CH$_3$SH)$_n^+$, $n \geq 3$, were nearly unobserved. An extra feature with $m/z = 94$, indicated as *, is due to impurity dimethyl disulfide (CH$_3$SSCH$_3$) that remained in the system after preceding experiments. The extremely weak signal at $m/z = 98$ is due to (CH$_3{}^{32}$SH)(CH$_3{}^{34}$SH).

In experimental condition B in which a stagnation pressure 3.3 atm for CH$_3$SH/Ne (1%) and a driving current of 100 A for the pulse valve were employed, (CH$_3$SH)$_2^+$ was also the

TABLE II. Comparison of experimental IR absorption wavenumbers in the SH-stretching modes with theoretical predictions.

(CH$_3$SH)$_n$	B3LYP/aug-cc-pVDZ		MP2/aug-cc-pVDZ			
n	Harmonic $\Delta\nu$[a]/cm^{-1}	I/I_1[b]	Harmonic[c]/cm^{-1}	Anharmonic[c]/cm^{-1}	I/I_1[b]	Experiment[d]/cm^{-1}
1		1.0	2753	2652	1.0[e]	2608
2						2601
(**2a**)	2.8	0.4	2746 (-7)	2646 (-6)	0.3	
	-64.6	23.3	2722 (-31)	2624 (-28)	8.9	
(**2b**)	-6.8	0.5	2749 (-4)	2647 (-5)	1.5	
	-7.6	2.1	2746 (-7)	2643 (-9)	0.5	
(**2c**)	-1.7	1.9	2747 (-6)	2647 (-5)	1.7	
	-1.7	0.0	2747 (-6)	2647 (-5)	0.0	
(**2d**)	-4.1	1.7	2749 (-4)	2646 (-6)	0.8	
	-4.4	0.2	2748 (-5)	2643 (-9)	0.5	
(**2e**)	2.8	0.6	2746 (-7)	2645 (-7)	1.1	
	-62.4	23.5	2705 (-48)	2608 (-44)	16.9	
3						2567
(**3a**)	-67.0	32.7				
	-67.0	32.7				
	-73.2	0.0				
(**3b**)	0.1	0.5				
	-75.6	42.5				
	-85.3	33.8				
(**3c**)	-58.8	27.3	2694 (-59)		31.9	
	-67.5	27.0	2674 (-79)		48.4	
	-87.2	24.6	2659 (-94)		24.3	
(**3d**)	-1.8	1.1				
	-63.2	31.2				
	-70.4	19.2				
(**3e**)	-2.4	0.6				
	-75.3	37.8				
	-86.7	32.2				
4						2567
5						2567
Reference	24			This work		this work

[a]Shifts from the monomer.
[b]IR intensity (I) relative to that (I_1) of the monomer.
[c]Shifts from the monomer are listed in parentheses.
[d]All values denote band maxima; the band origin of CH$_3$SH is 2605 cm^{-1}.
[e]IR intensity of CH$_3$SH is 1.8 km mol^{-1}.

TABLE III. Comparison of experimental IR absorption wavenumbers in the region 2800–3100 cm^{-1} with theoretical predictions of the CH-stretching modes.

$(CH_3SH)_n$ n	ν_2 Harmonic[a] /cm^{-1}	Anharmonic[a] /cm^{-1}	I[b]	ν_9 Harmonic[a] /cm^{-1}	Anharmonic[a] /cm^{-1}	I[b]	ν_1 Harmonic[a] /cm^{-1}	Anharmonic[a] /cm^{-1}	I[b]	Experiment[c] $2\nu_{10}$ /cm^{-1}	$2\nu_4$ /cm^{-1}	ν_2 /cm^{-1}	ν_1/ν_9 /cm^{-1}
1	3087	2966	23	3194	3048	6	3196	3048	5	2868	2895	2949	3014
2										2865	2890	2944	3010
(2a)	3086 (−1)	2963 (−3)	22	3193 (−1)	3046 (−2)	5	3197 (1)	3047 (−1)	4				
	3078 (−9)	2962 (−4)	18	3185 (−9)	3042 (−6)	2	3196 (0)	3044 (−4)	8				
(2b)	3082 (−5)	2963 (−3)	21	3191 (−3)	3044 (−4)	5	3197 (1)	3048 (0)	4				
	3081 (−6)	2961 (−5)	23	3189 (−5)	3044 (−4)	5	3195 (−1)	3047 (−1)	1				
(2c)	3081 (−6)	2965 (−1)	32	3189 (−5)	3045 (−3)	10	3196 (0)	3051 (3)	4				
	3080 (−7)	2964 (−2)	0	3189 (−5)	3045 (−3)	0	3195 (−1)	3050 (2)	0				
(2d)	3082 (−5)	2963 (−3)	22	3191 (−3)	3045 (−3)	4	3197 (1)	3048 (0)	1				
	3080 (−7)	2963 (−3)	22	3190 (−4)	3044 (−4)	4	3196 (0)	3047 (−1)	2				
(2e)	3080 (−7)	2963 (−3)	18	3189 (−5)	3044 (−4)	2	3195 (−1)	3049 (1)	3				
	3076 (−11)	2958 (−8)	25	3179 (−15)	3033 (−15)	9	3190 (−6)	3043 (−5)	6				
(3c)	3086 (−1)		22	3187 (−7)		7	3198 (2)		4	2859	2884	2942	3009
	3079 (−8)		17	3185 (−9)		4	3194 (−2)		4				
	3071 (−16)		20	3179 (−15)		5	3193 (−3)		4				
4										2857	2884	2940	3007
5										2856	2884	2938	3005

[a]Shifts from the monomer are listed in parentheses.
[b]IR intensity (I) in km mol^{-1}.
[c]All values denote band maxima; the band origins of CH$_3$SH are 2864 ($2\nu_{10}$), 2889 ($2\nu_4$), 2947 (ν_2), 3015 (ν_1), and 3012 (ν_9) cm^{-1}.

dominant species upon VUV ionization, but signals of a small proportion of $(CH_3SH)_n^+$, $n = 3$–5, were observed, as shown in Fig. 4(a). If we assume that the ionization efficiency of these clusters are similar, the observed relative ion intensities

yield approximately $[(CH_3SH)_2] : [(CH_3SH)_3] : [(CH_3SH)_4] : [(CH_3SH)_5] = 1.00 : 0.16 : 0.04 : 0.01$.

In experimental condition C in which a stagnation pressure 3.3 atm for CH$_3$SH/Ne (1%) and a driving current of 106 A for the pulse valve were employed, $(CH_3SH)_2^+$ was
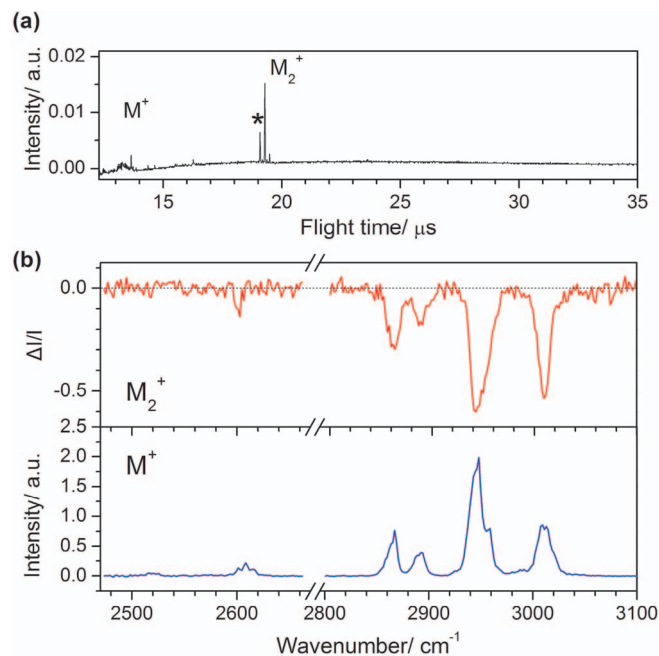

FIG. 3. Time-of-flight mass spectra (a) and action spectra (b) of a jet-cooled $(CH_3SH)_n$ cluster beam produced under the experimental condition A (see text). The action spectrum of $(CH_3SH)_2^+$, indicated as M$_2^+$, was recorded on monitoring the fractional variations in intensity of the ion signal; that of CH$_3$SH$^+$, indicated as M$^+$, was recorded on monitoring the increase in intensity as the wavelength of the IR laser was scanned. The peak indicated with * in (a) is due to impurity dimethyl disulfide.
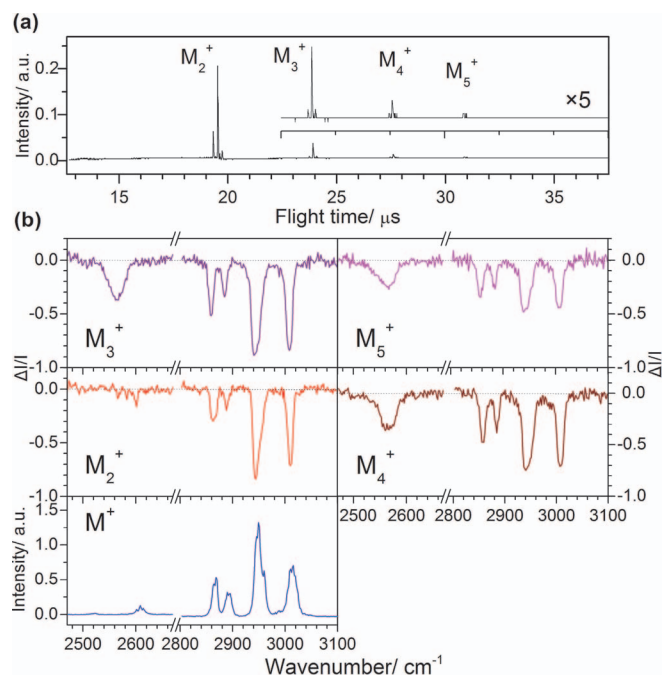

FIG. 4. Time-of-flight mass spectra (a) and action spectra (b) of a jet-cooled $(CH_3SH)_n$ cluster beam produced under the experimental condition B (see text). The action spectra of $(CH_3SH)_n^+$, indicated as M$_n^+$, $n = 2$–5, were recorded on monitoring the fractional variations in intensity of the ion signal as the wavelength of the IR laser was scanned. The spectrum of CH$_3$SH$^+$, indicated as M$^+$, was recorded on monitoring the increase in intensity.
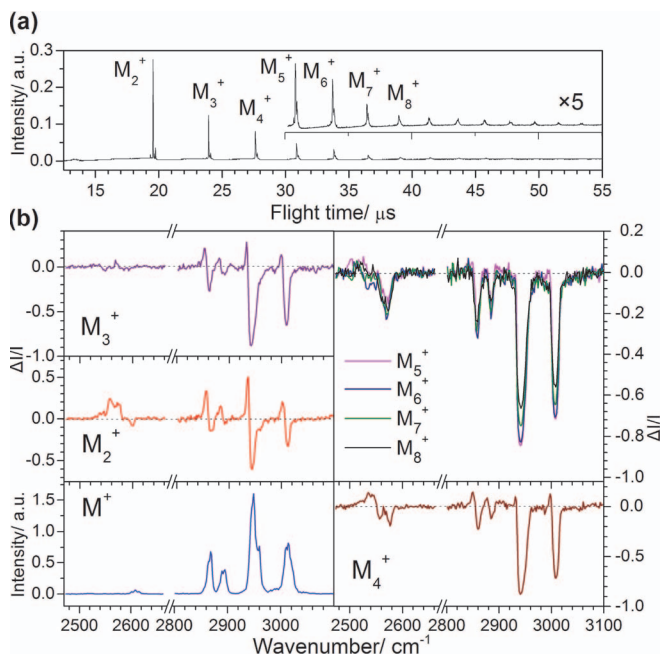
FIG. 5. Time-of-flight mass spectra (a) and action spectra (b) of a jet-cooled $(CH_3SH)_n$ cluster beam produced under the experimental condition C (see text). The action spectra of $(CH_3SH)_n^+$, indicated as M_n^+, $n = 2$–8, were recorded on monitoring the fractional variations in intensity of the ion signal as the wavelength of the IR laser was scanned. The spectrum of CH_3SH^+, indicated as M^+, was recorded on monitoring the increase in intensity.

still the most abundant species upon ionization, but concentrations of larger clusters were significant; cluster ions up to $(CH_3SH)_{15}^+$ were observed, as shown in Fig. 5(a). If we assume that the ionization efficiencies of these clusters are similar, the observed relative ion intensities yield approximately $[(CH_3SH)_2] : [(CH_3SH)_3] : [(CH_3SH)_4] : [(CH_3SH)_5] : [(CH_3SH)_6] : [(CH_3SH)_7] : [(CH_3SH)_8] = 1.00 : 0.44 : 0.28 : 0.13 : 0.09 : 0.04 : 0.02$.

In all experiments, the signal of CH_3SH^+ is small, indicating that fragmentation of $(CH_3SH)_2^+$ or larger clusters into CH_3SH^+ is unimportant. The variation of concentration of neutral $(CH_3SH)_n$ clusters upon IR irradiation is thus expected to be directly monitored through the variation in intensity of the $(CH_3SH)_n^+$ signal.

B. Action spectra upon tuning the IR wavelength

On monitoring simultaneously the intensity of each ion signal while scanning the wavelength of the IR laser, we recorded the action spectra that showed variations of the signal of each $(CH_3SH)_n^+$ cluster as a function of IR excitation wavenumber. For $(CH_3SH)_n^+$, $n \geq 2$, the observed signal was divided by the ion signal (I) recorded with no IR excitation then minus 1 to yield the fractional variation, indicated as $\Delta I/I$ in frame (b) of Figs. 3–5; $(CH_3SH)_n^+$ is indicated as M_n^+ in these figures. A negative value indicates a decrease whereas a positive value indicates an increase of concentration when these clusters were irradiated with the IR laser light. For CH_3SH^+, only the increase in intensity was plotted because the original signal was negligibly small in the absence of IR irradiation. These action spectra were recorded under

various experimental conditions in which varied distributions of methanethiol clusters were produced. Because no variation in ion signal was observed in the region 2670–2800 cm^{-1}, we show no spectra in this region to save space.

Under the experimental condition A, the significantly increased intensity of CH_3SH^+ shown in Fig. 3(b) is due to the IR-VUV (1+1) ionization of methanethiol monomer. In this case, some CH_3SH is excited to vibrationally excited levels of the ground electronic state on absorbing an IR photon before being ionized by the subsequent absorption of a VUV photon; the total energy of the IR and VUV photons, ~9.7 eV, exceeds the IE of CH_3SH, 9.446 eV.[36] The action spectrum obtained on monitoring $(CH_3SH)_2^+$, Fig. 3(b), shows only negative features in the 2470–3100 cm^{-1} region, indicating a net decrease of concentration of $(CH_3SH)_2$ upon IR irradiation because concentrations of larger ($n \geq 3$) clusters are extremely small; $(CH_3SH)_2$ produced from photodissociation of these larger clusters is consequently negligible.

Under the experimental condition B, we monitored the action spectra of $(CH_3SH)_n^+$, $n \leq 5$, as shown in Fig. 4(b). All action spectra of $(CH_3SH)_n^+$, $2 \leq n \leq 5$, show only negative features in the region 2470–3100 cm^{-1}, indicating that the destruction of $(CH_3SH)_m$ induced by IR photodissociation exceeded the production of $(CH_3SH)_m$ from larger clusters. The action spectra of $(CH_3SH)_n^+$, $3 \leq n \leq 5$, show five spectral features with one broad band near 2567 cm^{-1} and four in the region 2850–3050 cm^{-1}; their relative intensities and wavenumbers of bands are similar. In contrast, the action spectrum of $(CH_3SH)_2$ is similar to that recorded under the experimental condition A and lack the broad feature near 2567 cm^{-1}.

Under the experimental condition C, we monitored action spectra of $(CH_3SH)_n^+$, $n \leq 15$; only those of $(CH_3SH)_n^+$, $n \leq 8$ are shown in Fig. 5(b). In contrast to the experimental condition B, some positive features appear for $(CH_3SH)_n^+$, $2 \leq n \leq 4$. These features appear as the first-derivative of a positive absorption band, indicating the presence of a positive feature red-shifted from the negative feature with a similar band shape. In contrast, the action spectra of $(CH_3SH)_n^+$, $5 \leq n \leq 8$, are similar, with only negative features.

C. IR spectra of CH$_3$SH

The observed action spectra of M^+ in Figs. 3(b)–5(b) are nearly identical; they are expected to represent the IR spectrum of CH_3SH, if we assume that the ionization efficiencies for these vibrationally excited states are nearly identical at 132.50 nm. By comparison with the reported spectrum of gaseous CH_3SH,[37] the feature near 2608 cm^{-1} is assigned to the SH-stretching (ν_3) mode and those features near 2949 and 3014 cm^{-1} are assigned to the symmetric CH_3-stretching (ν_2) and the out-of-phase CH-stretching coupled with symmetric CH_2-stretching (ν_1)/ antisymmetric CH_2-stretching (ν_9) modes, respectively; the absorption bands of the ν_1 and ν_9 modes are too close to be resolved. The remaining features are due to overtone or combination bands: 2522 ($\nu_4 + \nu_6$), 2868 ($2\nu_{10}$), and 2895 cm^{-1} ($2\nu_4$).
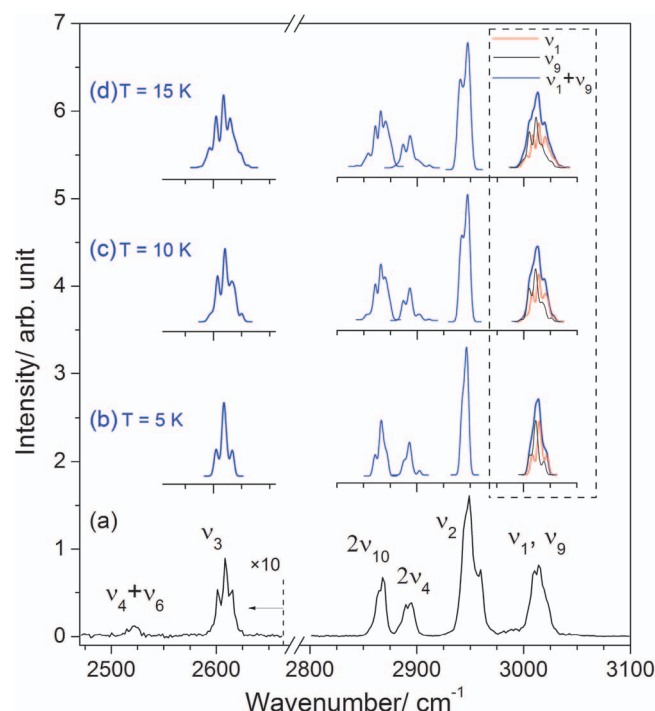
FIG. 6. (a) Comparison of simulated and observed IR spectra of jet-cooled CH_3SH. Spectrum recorded at resolution 2 cm^{-1} for the (1+1) photoionization spectrum of CH_3SH under the experimental condition A. (b)–(d) Spectra simulated with parameters: $J_{max} = 15$, $\nu_0 = 2605$ (ν_3), 2864 ($2\nu_{10}$), 2889 ($2\nu_4$), 2947 (ν_2), 3015 (ν_1), 3012 (ν_9) cm^{-1}, A'/A'', B'/B'', C'/C'', and hybrid type listed in Table I, and $T = 5$ K (b), 10 K (c), 15 K (d). The intensities of the simulated spectra are adjusted to match the experimental results.

We simulated the rotational contour of the absorption bands of CH_3SH with the SPECVIEW program[38] using predicted rotational parameters A', A'', B', B'', C', C'', $J_{max} = 15$, a Gaussian width (full width at half maximum) of 2 cm^{-1}, and a predicted hybrid ratio of a-type/b-type; the primes and double primes indicate the vibrationally excited and ground states, respectively. The predicted hybrid ratios of a-type/b-type, rotational parameters for the vibrational ground state and the excited states of each vibrational mode of CH_3SH were calculated with the MP2/aug-cc-pVDZ method, as listed in Table I. To minimize errors in calculated rotational parameters, we used the reported experimental rotational parameters of the equilibrium state A_e, B_e, and C_e (Ref. 39) and the calculated ratios of A/A_e, B/B_e, and C/C_e were used to simulate the observed spectra. Figure 6 compares the observed and spectra of several vibrational modes simulated at 5, 10, and 15 K; the best agreement was derived for $T \cong 10$ K and $\nu_3 = 2605$, $2\nu_{10} = 2864$, $2\nu_4 = 2889$, $\nu_2 = 2947$, $\nu_1 = 3015$, and $\nu_9 = 3012$ cm^{-1}, as shown in Fig. 6. The simulation of the symmetric CH_3-stretching (ν_2) mode agrees with the observed spectrum on the low-wavenumber side, but an additional component with maximum absorption near 2960 cm^{-1} cannot be accounted for by simulation of only the ν_2 band. This additional component might be due to the torsional splitting of this mode or an additional overlapping combination mode such as $\nu_7 + \nu_8 + \nu_{10}$ or $\nu_4 + \nu_7 + \nu_8$. For CH_3OH, the E and A$_1$ components of the CH-stretching (ν_2) mode were observed at 2994.6 and 3007.0 cm^{-1}, and the E and A$_2$

components of the antisymmetric CH_2-stretching (ν_9) mode were observed at 2952.0 and 2966.6 cm^{-1}; a negligibly small torsional splitting (0.05 cm^{-1}) was observed for the symmetric CH_3-stretching (ν_3) mode near 2844.7 cm^{-1}.[40,41] The observed separation of $\sim$13 cm^{-1} for ν_2 of CH_3SH is much larger than that of the corresponding (ν_3) mode of CH_3OH. We thus prefer the assignments of the additional feature to a combination mode.

Although we could not positively exclude the possibility that some vibrationally excited CH_3SH, produced from the fragmentation of larger clusters upon IR irradiation, might contribute to the observed spectrum of CH_3SH, we found no evidence of such contribution from the comparison of the observed spectrum with that simulated at 10 K.

D. IR spectra of $(CH_3SH)_2$

Upon IR irradiation, $(CH_3SH)_n$ dissociated into smaller clusters; the variation of the concentration of $(CH_3SH)_n$ led to the variation in the observed intensity of $(CH_3SH)_n^+$. We previously derived IR spectra of methanol clusters $(CH_3OH)_n$ from the action spectra on considering a simplified scheme for the dissociation and ionization of methanol clusters by assuming that, on absorption of an IR photon, methanol clusters $(CH_3OH)_n$ lose one methanol to become $(CH_3OH)_{n-1}$.[13] This scheme was based on the fact that the dissociation energies of $(CH_3OH)_n$, $n = 3–6$,[42,43] were predicted to be 0.4–0.6 eV so that, with original internal energy less than 0.2 eV for $(CH_3OH)_n$ in a supersonic jet, absorption of one infrared photon of energy 0.35–0.45 eV induces photodissociation of $(CH_3OH)_n$ to yield CH_3OH and $(CH_3OH)_{n-1}$, but is unlikely to eliminate two or more CH_3OH molecules.

For CH_3SH clusters, the dissociation energy is much smaller than that of CH_3OH clusters. The energy for $(CH_3SH)_3$ to dissociate one CH_3SH was calculated to be 0.07–0.18 eV depending on the method of calculation,[22,24] and that for $(CH_3SH)_4$ was predicted to be 0.124 eV with the MP2/aug-cc-pVDZ method.[22] The IR photon (0.31–0.38 eV) employed in this work is hence expected to dissociate more than one CH_3SH from the cluster. It is consequently difficult to employ a simple scheme such as that used for CH_3OH clusters[13] to obtain the spectra of $(CH_3SH)_n$ from observed action spectra. We have thus to rely on special experimental conditions to derive the spectra of $(CH_3SH)_n$.

As shown in Fig. 3(b), under the experimental condition A, the largest cluster ion in the TOF spectrum is $(CH_3SH)_2^+$, indicating that the largest cluster detectable in the supersonic jet was $(CH_3SH)_2$. The decrease of intensity of $(CH_3SH)_2^+$ upon IR irradiation is thus due to only the dissociation of $(CH_3SH)_2$. In Fig. 4(b), under the experimental condition B, the largest cluster ion in the TOF spectrum is $(CH_3SH)_5^+$, with intensities of $(CH_3SH)_3^+$, $(CH_3SH)_4^+$, and $(CH_3SH)_5^+$ 16, 4, and 1%, respectively, that of the most intense TOF signal of $(CH_3SH)_2^+$. The action spectrum of $(CH_3SH)_2^+$ shows no proportion of a positive signal and is nearly identical to the action spectrum of $(CH_3SH)_2^+$ recorded in the experimental condition A, indicating insignificant interference from the dissociation of the larger clusters. In contrast, the action

spectrum of $(CH_3SH)_2^+$ in Fig. 5(b) shows significant positive features that appear to be contributed from the dissociation of larger clusters. The band shape of first-derivative type with positive features in the low-energy region indicates that absorption of larger clusters is red-shifted from that of the smaller cluster. The negative of the action spectrum of $(CH_3SH)_2^+$ recorded under the experimental conditions A and B hence represent satisfactorily the IR absorption spectrum of $(CH_3SH)_2$.

The spectrum of $(CH_3SH)_2$ is similar to that of CH_3SH except for small red shifts. The SH-stretching (ν_3) mode was red-shifted by ~ 7 cm^{-1} from that (2608 cm^{-1}) of CH_3SH, in agreement with the predicted shifts for structures (**2b**), (**2c**), and (**2d**), as listed in Table II; as structures (**2a**) and (**2e**) have S–H$\cdots$S hydrogen-bonded structures, the proton donor has enhanced intensity and large (>30 cm^{-1}) shift from that of the monomer. The absence of a significantly red-shifted (>30 cm^{-1}) and intensity-enhanced band in the SH-stretching region indicates that the proportion of the dimer with the S–H$\cdots$S hydrogen-bond structure is insignificant. In the region 2850–3015 cm^{-1}, observed bands of $(CH_3SH)_2$ shift 3–5 cm^{-1} to the red of bands of CH_3SH to become 2865 ($2\nu_{10}$), 2890 ($2\nu_4$), 2944 (ν_2), and 3010 (ν_1/ν_9) cm^{-1}; the mode numbers of the monomer are listed in parentheses for reference. The width of the band near 2944 cm^{-1} increased and the intensity of the band near 3010 cm^{-1} was enhanced relative to those of CH_3SH. In this region, all structures of $(CH_3SH)_2$ were predicted to have small red shifts for ν_1, ν_2, and ν_9. For structures (**2a**) and (**2e**), the proton donor and proton acceptor show splitting, ~ 8 cm^{-1} for (**2a**) and 4–10 cm^{-1} for (**2e**), slightly larger than those (<2 cm^{-1}) for structures (**2b**)–(**2d**). Observed small shifts (3–5 cm^{-1}) agree more satisfactorily with those of (**2b**)–(**2d**). The observation agrees with the vibrational wavenumbers and IR intensities predicted for the most stable structure of $(CH_3SH)_2$, (**2b**), which contains no S–H$\cdots$S hydrogen bond. However, from the observed spectra, we could not positively exclude the possibility that structures (**2c**) and (**2d**) might also be present.

Our observation of $(CH_3SH)_2$ in the supersonic jet with dominant structures showing no S–H$\cdots$S hydrogen-bond is consistent with theoretical predictions that such structures have energies lower than those with the S–H$\cdots$S hydrogen-bond. This indicates that the S–H$\cdots$S hydrogen-bond is weak and the C–H$\cdots$S interactions between S and the methyl group prevails in $(CH_3SH)_2$. In contrast, the methanol dimer $(CH_3OH)_2$ shows an open-chain structure with nearly linear O–H$\cdots$O bond that is much stronger than the C–H$\cdots$O interaction.[13]

E. IR spectra of $(CH_3SH)_3$

In Fig. 4(b), the action spectrum of $(CH_3SH)_3^+$ recorded under the experimental condition B shows no apparent positive signal and is similar to the action spectrum of $(CH_3SH)_2^+$ in the 2800–3100 cm^{-1}, but an intense broad feature near 2567 cm^{-1} instead of a weak band near 2601 cm^{-1} is observed. In contrast, the action spectrum of $(CH_3SH)_3^+$ in Fig. 5(b) recorded under the experimental condition C shows
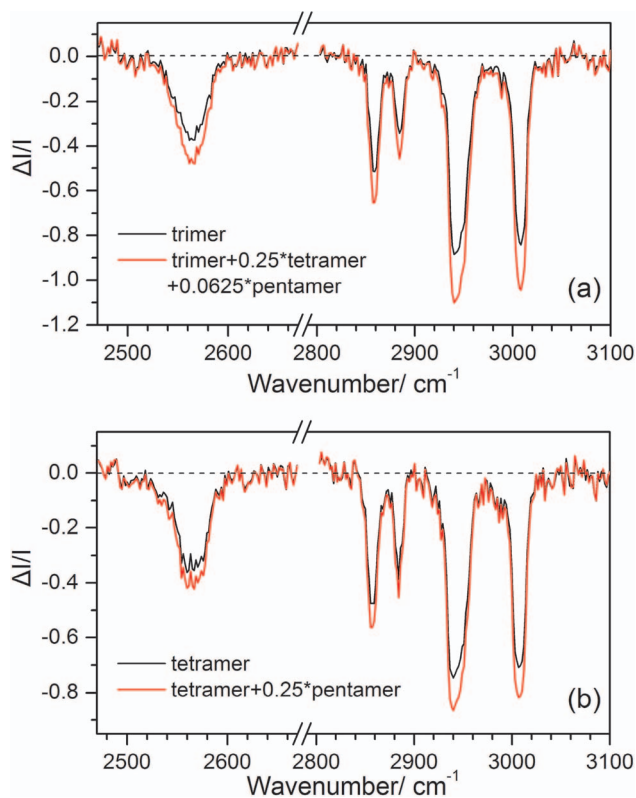

FIG. 7. (a) Comparison of the action spectrum of $(CH_3SH)_3^+$ under the experimental condition B and the revised action spectrum of $(CH_3SH)_3^+$ on assuming an extreme case in which all dissociated $(CH_3SH)_4$ and $(CH_3SH)_5$ leads to the formation of only $(CH_3SH)_3$. (b) Comparison of the action spectrum of $(CH_3SH)_4^+$ under the experimental condition B and the revised action spectrum of $(CH_3SH)_4^+$ on assuming an extreme case in which all dissociated $(CH_3SH)_5$ leads to formation of only $(CH_3SH)_4$.

positive features on the small-wavenumber side of each negative feature in the 2800–3100 cm^{-1} region; they are apparently due to formation of $(CH_3SH)_3$ from the dissociation of larger clusters. The near-zero change in intensity in the SH-stretching region might be due to a balance between destruction and formation of $(CH_3SH)_3$ in this wavelength region.

Under the experimental condition B, the dissociation of only $(CH_3SH)_4$ and $(CH_3SH)_5$ can contribute to the formation of $(CH_3SH)_3$. When we assumed an extreme case such that, upon irradiation with the IR light, all $(CH_3SH)_4$ and $(CH_3SH)_5$ that dissociate form $(CH_3SH)_3$, and took into account this contribution by assuming the absorption spectra of $(CH_3SH)_4$ and $(CH_3SH)_5$ to be the negative of the action spectra of the corresponding cluster ions, we obtained the absorption spectrum of $(CH_3SH)_3$, shown as the black trace in Fig. 7(a). In this correction, we assumed identical photoionization yields for all clusters and used the intensity factors relative to $(CH_3SH)_2^+$, 0.25 for $(CH_3SH)_3^+$, and 0.0625 for $(CH_3SH)_4^+$, observed in the TOF spectrum as the weighting factors for correction. We found no significant altered band shape in the resultant spectrum except a small modification of relative intensities. We hence conclude that the negative of the action spectrum of $(CH_3SH)_3^+$ recorded under the experimental condition B suitably represents the IR absorption spectrum of $(CH_3SH)_3$.

The spectrum of $(CH_3SH)_3$ is similar to that of $(CH_3SH)_2$ except a prominent broad feature near 2567 cm^{-1} and small red shifts in other bands; the weak feature near 2601 cm^{-1} for $(CH_3SH)_2$ was unobservable. The bands in region 2850–3015 cm^{-1} shift 5–11 cm^{-1} to the red from those of CH_3SH to become 2859 ($2\nu_{10}$), 2884 ($2\nu_4$), 2942 (ν_2), and 3009 (ν_1/ν_9) cm^{-1}; the mode numbers of the monomer are listed for the reference. The enhanced intensity and a large red (-41 cm^{-1}) shift of the SH-stretching (ν_3) mode are an indication of the existence of the S–H$\cdots$S hydrogen-bonded structure in $(CH_3SH)_3$. The absence of absorption of non-hydrogen-bonded SH moiety near 2608 cm^{-1} indicates that the major proportion of $(CH_3SH)_3$ has a cyclically hydrogen-bonded structure in which there is no "free" SH, similar to the cases of $(CH_3OH)_n$, $n = 3–6$.[13]

The reported vibrational wavenumbers for the hydrogen-bonded SH-stretching modes predicted with the B3LYP/aug-cc-pVDZ method for all structures (**3a**)–(**3e**) are red-shifted from that of the monomer by 59–87 cm^{-1}; the intensities are enhanced 19–43 times those of the monomer.[24] Our observation of a broad feature with a maximum at 2567 cm^{-1} indicates a red shift of 41 cm^{-1} from the CH_3SH, slightly smaller than prediction but within expected uncertainties. The structures (**3b**) and (**3c**) are predicted to be the most stable and have similar energies; structure (**3c**) has a cyclic network of hydrogen bonds, whereas structure (**3b**) has one S–H bond with no hydrogen bond. The predicted spectrum of structure (**3c**) is consistent with our observation, but we cannot positively exclude the existence of other structures that have one non-hydrogen-bonded SH moiety based on the absence of a band near 2608 cm^{-1} because these "free" SH-stretching bands were predicted to have much smaller IR intensity.

The predicted vibrational wavenumbers of the hydrogen-bonded SH-stretching modes vary by 6.2, 9.7, 28.4, 7.2, and 11.4 cm^{-1} for structures (**3a**)–(**3e**), respectively. Observed half-width of 35 cm^{-1} for the band at 2567 cm^{-1} agrees better with that expected for structure (**3c**) that has a variation in wavenumbers of SH-stretching modes much larger than those of other structures.

As previous authors reported no prediction of the vibrational wavenumbers of the CH-stretching modes, we performed calculations on the most stable structure (**3c**) with the MP2/aug-cc-pVDZ method, as listed in Table III. The predicted harmonic vibrational wavenumbers of ν_2, ν_9, and ν_1 are red-shifted by 1–16, 7–15, and (-2)–3 cm^{-1}, respectively, from CH_3SH, with their IR intensities similar to those of the corresponding modes of CH_3SH. The observed red shifts of 7 and 5 cm^{-1} with widths $\sim$20 and 15 cm^{-1} for ν_2 and ν_9/ν_1 bands, respectively, are smaller than, but consistent with, predictions. In summary, the observed spectrum of $(CH_3SH)_3$ agrees best with that predicted for structure (**3c**).

Our observation of $(CH_3SH)_3$ with dominant structures showing S–H$\cdots$S hydrogen-bonds, likely with a cyclic structure, is consistent with theoretical predictions that the more stable structures of $(CH_3SH)_3$ have cyclic S–H$\cdots$S hydrogen-bonds.[24] This indicates that the S–H$\cdots$S hydrogen-bond is more important than the C–H$\cdots$S interactions in $(CH_3SH)_3$, suggesting the presence of cooperative phenomenon, similar to the case of $(CH_3OH)_3$.[13] According-

ing to theoretical calculations, the contribution of nonadditive pairwise terms to the interaction was small ($\sim$6% of the overall interaction energy) but significant.[24] The presence of additional C–H$\cdots$S interactions between S atoms and CH_3 groups also helps to stabilize the cluster, and this defies a clear analysis of the contributions of each type of interaction.

F. IR spectra of $(CH_3SH)_n$, $n = 4$ and 5

Because $(CH_3SH)_5{}^+$ is the largest cluster ion that we observed in the time-of-flight spectrum under the experimental condition B (Fig. 4), we expect that the negative of the recorded action spectrum of $(CH_3SH)_5{}^+$ represents the IR absorption spectrum of $(CH_3SH)_5$. The contribution from the absorption of $(CH_3SH)_5$ to the action spectrum of $(CH_3SH)_4{}^+$ is expected to be small because the signal of $(CH_3SH)_5{}^+$ is only one quarter that of $(CH_3SH)_4{}^+$, especially as $(CH_3SH)_5$ likely decomposes to form $(CH_3SH)_n$, $n \leq 3$ upon IR irradiation. When we assume an extreme case that, upon irradiation of the IR light, all dissociated $(CH_3SH)_5$ forms $(CH_3SH)_4$ and take into account this effect by using the negative of the action spectra of $(CH_3SH)_5{}^+$ as the absorption spectrum of $(CH_3SH)_5$, we found no significantly altered band shape in the resultant spectrum except a small modification of relative intensities, as shown in Fig. 7(b). We hence conclude that the negative of the action spectra of $(CH_3SH)_4{}^+$ and $(CH_3SH)_5{}^+$ recorded under the experimental condition B properly represent the IR absorption spectra of $(CH_3SH)_4$ and $(CH_3SH)_5$. The observed bands are at 2567, 2857, 2884, 2940, and 3007 cm^{-1} for $(CH_3SH)_4$ and 2567, 2856, 2884, 2938, and 3005 cm^{-1} for $(CH_3SH)_5$. We compare the absorption spectra of $(CH_3SH)_n$, $n = 1–5$, in Fig. 8; the dashed lines help to identify the small shifts among clusters of varied size. The absorption maxima are also summarized in Table II (for SH-stretching) and Table III (for CH-stretching region).

Neither experimental, nor theoretical vibrational wavenumber of $(CH_3SH)_4$ and $(CH_3SH)_5$ has been reported. Our observation of a broad feature with maximum near 2567 cm^{-1} (41 cm^{-1} red shifted from the monomer) and half-widths of 35 and 42 cm^{-1} for $(CH_3SH)_4$ and $(CH_3SH)_5$, respectively, are similar to that of $(CH_3SH)_3$, except a slightly wider and red-degraded band shape for the SH-stretching mode of $(CH_3SH)_5$. If this red shift is due to a cooperative effect, it is much smaller than that in the CH_3OH clusters in which the OH-stretching band of $(CH_3OH)_5$ was red-shifted 443 cm^{-1} from CH_3OH and the width increased from $\sim$50 cm^{-1} for CH_3OH to $\sim$300 cm^{-1} for $(CH_3OH)_5$. The observed red shifts of 9 and 11 cm^{-1} for the ν_2 band, 7 and 9 cm^{-1} for the ν_9/ν_1 band of $(CH_3SH)_4$ and $(CH_3SH)_5$, respectively, are small but significant.

G. IR spectra of $(CH_3SH)_n$, $n \geq 6$

The spectra of $(CH_3SH)_n$, $n \geq 6$ have to be derived from experiments under condition C (Fig. 5). In this experiment, because the cluster size is as large as $n = 15$ and the size distribution follows a smooth curve, to derive their spectra by assuming a simple dissociation mechanism is difficult.
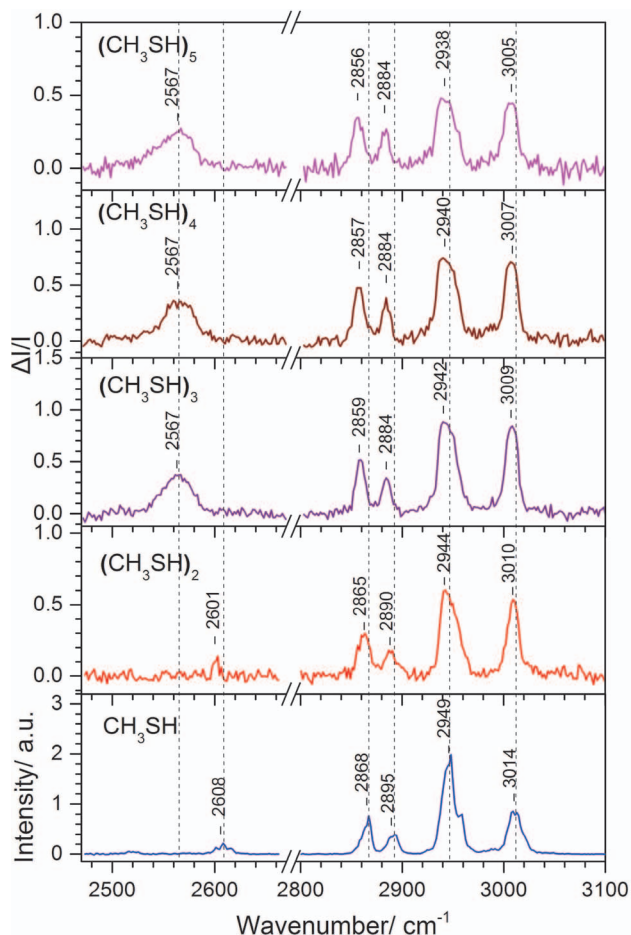
FIG. 8. Comparison of IR absorption spectra of $(CH_3SH)_n$, $n = 1$–5, in region 2470–3100 cm^{-1}. The listed wavenumbers are band maxima. The dashed lines facilitate the recognition of small spectral shifts.

Although the action spectra of $(CH_3SH)_n$, $n = 2$–4, in Fig. 5 show some positive features, those of $(CH_3SH)_n$, $n \geq 5$, have insignificant positive features, indicating that either the absorption spectra of the larger clusters are similar to those of the smaller clusters or the contributions from the dissociations of larger clusters are insignificant. We plot the action spectra of $(CH_3SH)_n$, $n = 5$–8, in Fig. 5 to illustrate that these spectra are similar in both band positions and shapes, and vary only slightly in relative intensities. We thus conclude that the absorption spectra of $(CH_3SH)_n$, $5 \leq n \leq 8$ are similar.

V. CONCLUSION

We investigated IR absorption in the 2470–3100 cm^{-1} region of size-selected methanethiol clusters, $(CH_3SH)_n$ with $2 \leq n \leq 5$, in a pulsed supersonic jet using IR-VUV ionization and TOF mass detection. From the observed action spectra under various experimental conditions, we obtained IR spectra of size-selected $(CH_3SH)_n$, $n = 2$–5. In the SH-stretching region, $(CH_3SH)_2$ has a weak absorption band at ~2601 cm^{-1}, similar to the band at ~2608 cm^{-1} of CH_3SH, whereas $(CH_3SH)_n$, $n \geq 3$, have an intense broad feature near 2567 cm^{-1}. This observation indicates that the S–H$\cdots$S hydrogen bonding occurs only for $(CH_3SH)_n$, $n \geq 3$, but is insignificant for $(CH_3SH)_2$, consistent with theoretical predic-

tions. The absence of a band near 2608 cm^{-1} and the large width of the feature near 2567 cm^{-1} for $(CH_3SH)_n$, $n \geq 3$ indicate that the S–H$\cdots$S hydrogen-bonded structure is mainly cyclic. The spectra in the CH-stretching region are similar for all clusters, except for small red shifts as the cluster-size increases, indicating the insignificant contribution from the methyl moiety in the bonding of the clusters.

[1]T. S. Zwier, Annu. Rev. Phys. Chem. **47**, 205 (1996).
[2]J. J. Scherer, J. B. Paul, A. O'Keefe, and R. J. Saykally, Chem. Rev. **97**, 25 (1997).
[3]W. H. Robertson and M. A. Johnson, Annu. Rev. Phys. Chem. **54**, 173 (2003).
[4]U. Buck and F. Huisken, Chem. Rev. **100**, 3863 (2000).
[5]M. A. Suhm, Adv. Chem. Phys. **142**, 1 (2009).
[6]T. Häber, U. Schmitt, and M. A. Suhm, Phys. Chem. Chem. Phys. **1**, 5573 (1999).
[7]R. W. Larsen, P. Zielke, and M. A. Suhm, J. Chem. Phys. **126**, 194307 (2007).
[8]R. W. Larsen and M. A. Suhm, J. Chem. Phys. **125**, 154314 (2006).
[9]R. A. Provencal, J. B. Paul, K. Roth, C. Chapo, R. N. Casaes, R. J. Saykally, G. S. Tschumper, and H. F. Schaefer III, J. Chem. Phys. **110**, 4258 (1999).
[10]R. A. Provencal, R. N. Casaes, K. Roth, J. B. Paul, C. N. Chapo, R. J. Saykally, G. S. Tschumper, and H. F. Schaefer III, J. Phys. Chem. A **104**, 1423 (2000).
[11]H. B. Fu, Y. J. Hu, and E. R. Bernstein, J. Chem. Phys. **124**, 024302 (2006).
[12]Y. J. Hu, H. B. Fu, and E. R. Bernstein, J. Chem. Phys. **125**, 154306 (2006).
[13]H.-L. Han, C. Camacho, H. A. Witek, and Y.-P. Lee, J. Chem. Phys. **134**, 144309 (2011).
[14]L. J. M. Manojlović-Muir, Nature (London) **224**, 686 (1969), and reference therein.
[15]S. Mukherjee, S. R. Palit, and S. K. De, J. Phys. Chem. **74**, 1389 (1970), and references therein.
[16]H. S. Biswal, P. R. Shirhatti, and S. Wategaonkar, J. Phys. Chem. **113**, 5633 (2009).
[17]H. S. Biswal, P. R. Shirhatti, and S. Wategaonkar, J. Phys. Chem. **114**, 6944 (2010).
[18]See http://toxnet.nlm.nih.gov/cgi-bin/sis/htmlgen?HSDB for Hazardous Substances Data Bank [Internet]; Bethesda (MD): National Library of Medicine (US); Methyl Mercaptan; Hazardous Substances Databank Number: 813.
[19]A. J. Barnes, H. E. Hallam, and J. D. R. Howells, J. Chem. Soc., Faraday Trans. **68**, 737 (1972).
[20]J. A. Odutola, R. Viswanathan, and T. R. Dyke, J. Am. Chem. Soc. **101**, 4787 (1979).
[21]K. Pecul and R. Janoschek, Theor. Chim. Acta **36**, 25 (1974).
[22]A. K. Sum and S. I. Sandler, J. Phys. Chem. A **104**, 1121 (2000).
[23]I. Bakó and G. Pálinkás, J. Mol. Struct.: THEOCHEM **594**, 179 (2002).
[24]E. M. Cabaleiro-Lago and J. Rodríguez-Otero, J. Phys. Chem. A **106**, 7440 (2002).
[25]C. Morgado, M. A. Vincent, I. H. Hillier, and X. Shan, Phys. Chem. Chem. Phys. **9**, 448 (2007).
[26]Y. Matsuda, N. Mikami, and A. Fujii, Phys. Chem. Chem. Phys. **11**, 1279 (2009).
[27]Y. Matsuda, M. Mori, M. Hachiya, A. Fujii, and N. Mikami, Chem. Phys. Lett. **422**, 378 (2006).
[28]D. Sakai, Y. Matsuda, M. Hachiya, M. Mori, A. Fujii, and N. Mikami, J. Phys. Chem. A **112**, 6840 (2008).
[29]Y. J. Hu, H. B. Fu, and E. R. Bernstein, J. Chem. Phys. **125**, 154305 (2006).
[30]Y. J. Hu, H. B. Fu, and E. R. Bernstein, J. Chem. Phys. **125**, 154308 (2006).

[31] H.-L. Han, L. Fu, and Y.-P. Lee, Chem. Phys. Lett. **515**, 1 (2011).

[32] M. J. Frisch, G. W. Trucks, H. B. Schlegel *et al.*, GAUSSIAN 09, Revision C.2, Gaussian Inc., Wallingford, CT, 2009.

[33] T. H. Dunning, Jr., J. Chem. Phys. **90**, 1007 (1989).

[34] D. E. Woon and T. H. Dunning, Jr., J. Chem. Phys. **98**, 1358 (1993).

[35] L. A. Curtiss, K. Raghavachari, P. C. Redfern, V. Rassolov, and J. A. Pople, J. Chem. Phys. **109**, 7764 (1998).

[36] S. Nourbakhsh, K. Norwood, H.-M. Yin, C.-L. Liao, and C. Y. Ng, J. Chem. Phys. **95**, 946 (1991).

[37] I. W. May and E. L. Pace, Spectrochim. Acta A **24**, 1605 (1968).

[38] V. Stakhursky and T. A. Miller, "SPECVIEW: Simulation and Fitting of Rotational Structure of Electronic and Vibronic Bands," in *Proceedings of the 56th OSU International Symposium on Molecular Spectroscopy*, Columbus, OH USA, 2001; also available at http://www.chemistry.ohio-state.edu/~vstakhur.

[39] L. B. Fiona, K. V. L. N. Sastry, H. Eric, A. Sieghard, C. O. Lee, and C. D. L. Frank, Astrophys. J. **510**, 789 (1999).

[40] L.-H. Xu, X. Wang, T. J. Cronin, D. S. Perry, G. T. Fraser, and A. S. Pine, J. Mol. Spectrosc. **185**, 158 (1997).

[41] X. Wang and D. S. Perry, J. Chem. Phys. **109**, 10795 (1998).

[42] U. Buck, J.-G. Siebers, and R. J. Wheatley, J. Chem. Phys. **108**, 20 (1998).

[43] F. C. Hagemeister, C. J. Gruenloh, and T. S. Zwier, J. Phys. Chem. A **102**, 82 (1998).